AIAA JOURNAL
Vol. 45, No. 3, March 2007

Characterization of the Microfluidic Oscillator

James W. Gregory* and John P. Sullivan†
Purdue University, West Lafayette, Indiana 47907
Ganesh Raman‡
Illinois Institute of Technology, Chicago, Illinois 60616
and
Surya Raghu§
Advanced Fluidics Corporation, Ellicott City, Maryland 21042

DOI: 10.2514/1.26127

The microfluidic oscillator is a new microscale actuator developed for flow control applications. These patented devices can produce a 325-μm-wide oscillating gas jet at high frequencies (over 22 kHz) and very low flow rates ($\sim$1 l/min or $\sim$1 g/min). Furthermore, microfluidic oscillators have no moving parts; the jet oscillations depend solely on the internal fluid dynamics. In this work, the flowfield of a microfluidic oscillator is characterized using pressure transducers, water visualization, and pressure-sensitive paint. The acoustic field and frequency spectrum were characterized for the oscillator at several flow rates. The results indicate that the external flowfield of the microfluidic oscillator is marked by two distinct operating regimes, separated by a transitional increase in turbulent noise. This work also demonstrates a significant advance in pressure-sensitive paint technology. New instrumentation was developed to resolve small-scale, time-resolved measurements of a high-frequency micro flowfield. A macro imaging system was used to provide a spatial resolution of approximately 3 mm per pixel and time-resolved, full-unsteady pressure measurements at oscillation frequencies up to 21 kHz.

I. Introduction

FLOW control actuators are devices that are used to enact large-scale changes in a flowfield with a relatively small input. Often these changes are focused on improving the performance of a flight vehicle by delaying stall, reducing drag, enhancing lift, abating noise, reducing emissions, etc. In many flow control situations, unsteady actuation is required for optimal performance. Unsteady actuators are particularly beneficial in closed-loop control applications when the frequency of the unsteady actuation can be directly controlled. Common flow control actuators include synthetic jets [1], piezoelectric benders [2,3], powered resonance tubes (also known as Hartmann whistles) [4–6], plasma actuators [7–10], pulsed jets [11–13], and steady blowing [14] or suction [15]. These devices and concepts all have inherent strengths and some limitations. Thus, the selection of a flow control actuator often is driven by the requirements of the application. A new small-scale flow control actuator is introduced in this paper: the microfluidic oscillator. This particular actuator has the advantages of high-frequency bandwidth, low mass flow requirements, and simplicity. Because the microfluidic oscillator is a new device, its flowfield has not yet been characterized. This paper focuses on studying the flowfield of the oscillator with advanced measurement techniques. A second objective of this work is to demonstrate the superior frequency response characteristics and fine spatial resolution of porous pressure-sensitive paint (PSP).

A. Fluidic Oscillator

The fluidic oscillator is a device that produces an oscillating jet when supplied with a pressurized fluid, as shown in the example schlieren images in Fig. 1. The fluidic oscillator has its roots based in the field of fluid logic, as detailed by Morris [16], and Kirshner and Katz [17]. A comprehensive overview of the fluid amplifier technology and an extensive bibliography may be found in the NASA contractor reports edited by Raber and Shinn [18,19]. Fluid logic principles were first applied by Spyropoulos [20] to create a self-oscillating fluidic device. Viets [21] also published early work concerning the development of fluidic oscillators. Since then, fluidic oscillators have been used for a wide variety of applications, including windshield washer fluid nozzles [22], flow rate metering [23,24], and flow control applications.

The fluidic oscillator represents a useful device for flow control applications because of its variable frequency, the unsteady nature of the oscillating jet, the wide range of dynamic pressures possible, and the simplicity of its design. A very attractive feature of fluidic oscillators is that they have no moving parts; the simple design of the fluidic oscillator produces an oscillating jet based solely on internal fluid dynamic interactions. Flow control applications of the fluidic oscillator have included cavity resonance tone suppression [25,26], enhancement of jet mixing [27–29], jet thrust vectoring [30], and separation control [31].

There has been a substantial amount of prior work to characterize the flow of fluidic oscillators, including miniature fluidic oscillators. Raman et al. [32] and Raghu and Raman [33] have characterized miniature fluidic oscillators as possible candidates for flow control applications. Sakaue et al. [34] and Gregory et al. [35–37] have used pressure-sensitive paint to characterize the flow of miniature fluidic oscillators. Gregory et al. [38] investigated the mode of operation of the fluidic oscillator by studying the internal fluid dynamics of the device. In that work, the exact same design as the current micro oscillator was used, only on a larger scale.

The microfluidic oscillators characterized in these tests are unique in three aspects. These actuators require very low flow rates, typically 450–1100 ml/min. In addition, the size of the oscillating jet is on the

Presented as Paper 2692 at the 2nd AIAA Flow Control Conference, Portland, OR, 28 June–1 July 2004; received 24 June 2006; accepted for publication 2 November 2006; revision received 29 November 2006.

*Doctoral Fellow, School of Aeronautics and Astronautics, 315 North Grant Street, currently National Research Council (NRC) Postdoctoral Research Fellow at the U.S. Air Force Academy, 2410 Faculty Drive, Suite 106, USAF Academy, CO 80840; jim.gregory@alumni.purdue.edu. Member AIAA.

†Professor, School of Aeronautics and Astronautics, 315 North Grant Street, Senior Member AIAA.

‡Associate Professor, Department of Mechanical, Materials and Aerospace Engineering, 10 West 32nd Street. Associate Fellow AIAA.

§President, 4217 Red Bandana Way. Associate Fellow AIAA.

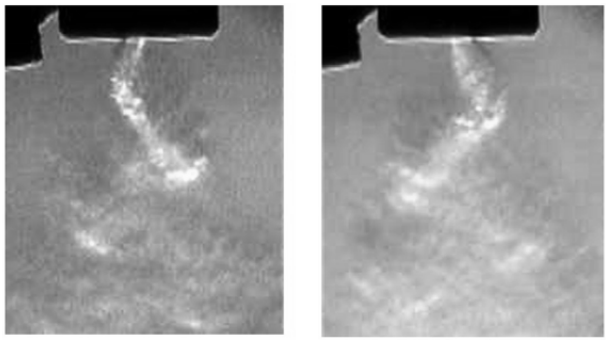

a) b)

Fig. 1 Schlieren images of typical jet oscillations of a miniature fluidic oscillator: a) 0-deg phase and b) 180-deg phase.

microscale, approximately 325 μm in diameter. The jet produced by the microfluidic oscillator has a much higher oscillation frequency than the miniature fluidic oscillator. The typical range of oscillation frequency for the microfluidic oscillator is from 6 kHz up to over 22 kHz. As will be shown in this work, a distinctive feature of the microfluidic oscillator is that the jet of air is spatially modulated, in contrast with a jet modulated solely in time. This provides a wider region of impact in a flowfield of interest. These design features (low flow rate, high frequency, and spatial modulation) make the microfluidic oscillator an attractive candidate actuator for aerospace applications such as separation control. The fluidic oscillator can be used to spatially and temporally modulate a steady jet to enhance the effectiveness of blowing for flow control applications. This can be accomplished with no added system complexity, with the only penalty being higher pressure losses. The design of the microfluidic oscillator evaluated in these tests follows the principles detailed in Raghu's patent [39]. The oscillator operates without feedback tubes; the unsteady interaction of two colliding fluid jets inside a mixing chamber, along with oscillatory growth and decay of opposing vortices, causes the oscillatory motion of the issuing jet (Gregory et al. [38]).

B. Pressure-Sensitive Paint

Pressure-sensitive paint is a key measurement technique employed for the results presented in this paper. PSP measures surface pressure distributions through the processes of luminescence and oxygen quenching. A diagram summarizing the PSP technique is shown in Fig. 2. Typically, PSP is illuminated with an excitation light, which causes luminophore molecules in the paint to luminesce. In the presence of oxygen in a test gas, the luminescent intensity of the luminophore is reduced through a transfer of energy from the luminophore to the oxygen molecules, a process known as oxygen

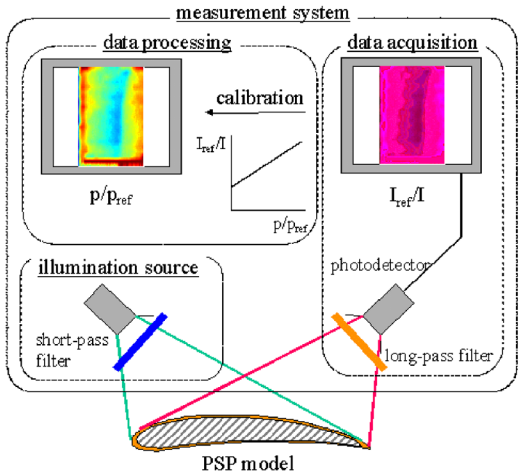

Fig. 2 Method of data acquisition and reduction for pressure-sensitive paint (Sakaue [44]).

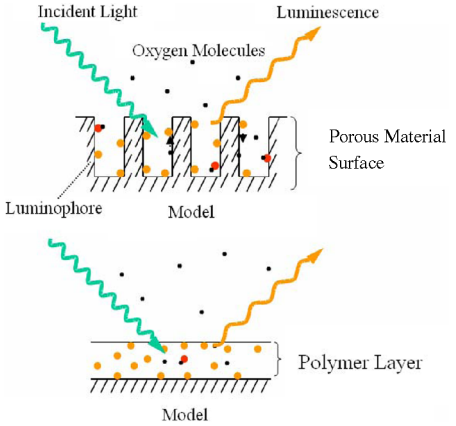

Fig. 3 Comparison of porous PSP with conventional PSP (Sakaue et al. [34]).

quenching. Because the amount of oxygen is proportional to air pressure, one can obtain static pressure levels from the change in the luminescent intensity of PSP, with intensity being inversely proportional to pressure. Pressure-sensitive paint was initially proposed as a qualitative flow-visualization tool [40] and was subsequently developed as a quantitative technique [41]. The accuracy and utility of PSP has improved such that the technique provides results that complement data obtained from conventional pressure instrumentation. Comprehensive reviews of the PSP technique have been published by Bell et al. [42] and Liu and Sullivan [43].

The PSP formulation traditionally used for conventional testing includes a polymer binder, which attaches the luminophore to the model surface. Conventional polymer-based PSPs are limited in response time, however. The slow response time characteristic of conventional PSP makes it a limited tool in the measurement of unsteady flowfields. Therefore, a fast responding paint, such as porous PSP, is needed for application to unsteady flow.

Porous PSP uses an open, porous matrix as a PSP binder, which improves the oxygen diffusion process. Figure 3 schematically describes the difference between conventional polymer-based PSP and porous PSP. For conventional PSP, oxygen molecules in a test gas need to permeate into the binder layer for oxygen quenching. The process of oxygen permeation in a polymer binder layer produces slow response times for conventional PSP. On the other hand, the luminophore in porous PSP is opened to the test gas so that the oxygen molecules are free to interact with the luminophore. The open binder provides much higher surface area, creating a PSP that responds much more quickly to changes in oxygen concentration and, thus, pressure.

There are three main types of porous pressure-sensitive paints currently in use, depending on the type of binder used. Anodized aluminum PSP (AA-PSP) [44–49] uses anodized aluminum as a porous PSP binder. Anodized aluminum is created through an electrochemical process by etching small pores (~10-nm diameter) on an aluminum surface. The luminophore is deposited directly on the porous surface by chemical and physical adsorption. Anodized aluminum is regarded as providing the fastest PSP response times, but is limited by the choice of material and cannot be sprayed onto a model. Thin-layer chromatography PSP (TLC-PSP) uses a commercial porous silica thin-layer chromatography (TLC) plate as the binder [50]. TLC plates are commonly used in chemistry laboratories and are composed of a thin layer (~250 μm) of silica gel. The disadvantages of the thin-layer chromatography plate are that it is fragile and limited to simple shapes. Polymer/ceramic PSP (PC-PSP) is a hybrid, porous binder that uses a small amount of polymer with a large amount of hard ceramic particles [51–53]. The resulting aggregate is a highly porous surface that allows for rapid diffusion. The primary advantage of polymer/ceramic PSP is that it may be sprayed on a model and offers reasonable response times. For each of these porous surfaces, the luminophore is applied directly by dipping or spraying.

Before using porous pressure-sensitive paint for an unsteady flowfield such as the microfluidic oscillator, it is important to characterize the unsteady response of the paint. Previous work by Sakaue et al. [34,48] and Gregory et al. [35–37,54] demonstrate that porous PSP has a flat frequency response in excess of 40 kHz. Furthermore, Asai et al. [55] have performed tests with anodized aluminum PSP in a shock tube and have shown step response times of the order of 1.8 μs. The proven response characteristics of the paint make it a suitable measurement technique for the flowfield of the microfluidic oscillator, which has a characteristic frequency of the order of tens of kilohertz.

This work relies on the fast response characteristics of porous PSP formulations to make time-resolved measurements of the fluidic oscillator flow. Anodized aluminum is the paint sample selected for use in the current study, primarily because of its superior frequency response characteristics. The oscillations are of the order of 21 kHz, making this one of the fastest flowfields measured with porous PSP to date. In addition, macro imaging techniques are employed to obtain sufficient spatial resolution. These tests are based on the work of Huang et al. [56], who employed macro imaging techniques to obtain a spatial resolution of the order of 3 μm.

II. Experimental Setup

The oscillation frequency of the microfluidic oscillator was characterized with a Kulite pressure transducer (XCS-062) or, in some cases, a miniature electret microphone. The pressure transducer was mounted in the near field of the oscillator flow, approximately 10 jet diameters away from the jet exit and in the same plane as the range of jet oscillations (but outside the flow). This location and orientation were selected to provide a clean signal for triggering the data acquisition timing, and the position was also constrained by the presence of the sample of pressure-sensitive paint. The physical location and orientation of the Kulite pressure transducer are shown in Fig. 4. When microphone measurements were recorded, the microphone was positioned in the acoustic far field, at an angle of 45 deg to the plane of oscillations and approximately 100 jet diameters away from the jet exit. The microphone and pressure transducer data provide frequency data for comparison with the pressure-sensitive paint results and also provide a timing reference for phase-locking the PSP data acquisition. It is important to note that both the Kulite pressure transducer and the microphone were positioned *outside* the jet flowfield. Thus, both of these transducers measured the *acoustic* pressure fluctuations resulting from the jet oscillations. The signal from the pressure transducer or the microphone was digitized with a National Instruments BNC-2080 board and AI-16E-4 DAQ card, with a sampling rate of 250 kHz. The flow rate of the fluidic oscillator was measured with an Omega FL-3600 Rotameter, and the pressure was measured with a digital pressure transducer.

The experimental setup of the microfluidic oscillator with PSP instrumentation is shown in Fig. 4. Anodized aluminum pressure-sensitive paint was used as the PSP formulation for these tests. The anodized aluminum surface was prepared according to Sakaue's procedure [44], and the luminophore employed was tris (bathophenanthroline) ruthenium dichloride, $(C_{24}H_{16}N_2)_3RuCl_2$ from GFS Chemicals (CAS # 36309-88-3). Nitrogen was used as the test gas in these experiments, because it purges atmospheric oxygen and provides high-contrast data from the oxygen-sensitive PSP. The paint sample was positioned parallel to the jet flow exiting the microfluidic oscillator, as shown in Fig. 4. The paint sample was precisely positioned such that there was minimal impact on the flowfield of the issuing jet, but still allowing for effective measurement of the jet oscillations. Interference effects are considered negligible because the presence of the paint sample does not alter the frequency of oscillations for a given pressure condition, nor does it alter the flow rate or pressure conditions.

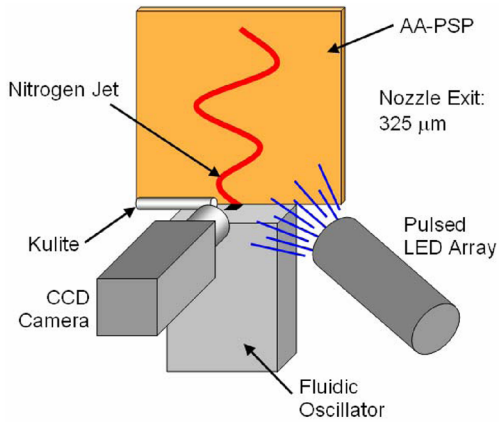

Fig. 4 Experimental setup for the pressure-sensitive paint measurements.

The imaging system consisted of a CCD camera, a bellows assembly, a reversed lens, and a long-pass optical filter. A 12-bit Photometrics SenSys CCD camera with 512 × 768 pixel resolution was used for imaging. A Nikon PB-6 bellows was used to extend the lens from the image plane, with the extension set at approximately 200 mm. A 50-mm *f*1.8 Nikon lens was reversed and mounted on the bellows with a Nikon BR-2A lens reversing ring. A 590-nm long-pass filter (Schott Glass OG590) was used for filtering out the excitation light and was attached to the lens bayonet mount with a Nikon BR-3 filter adapter ring.

A pulsed array of 48 blue LEDs (OptoTech, Shark Series) was used for excitation of the PSP. This LED array removes the individual LED packaging and mounts the individual dies in a TO-66 package, creating a compact unit. The excitation light was filtered with an Oriel 58879 short-pass filter. For full-field imaging, the camera shutter must be left open for an extended period (typically, several seconds) to integrate enough light for quality images. Therefore, the pulsing of the excitation light was phase-locked with the oscillation of the microfluidic oscillator to capture one point in the oscillation cycle. The strobe rate was synchronized with the signal from the pressure transducer mounted in the near field of the oscillator flow. The Kulite signal was passed to an oscilloscope with a gate function. The gate function produced a TTL pulse with a width corresponding to the time the scope was triggered. Thus, the oscilloscope was used to generate a once-per-cycle TTL pulse. This TTL signal from the oscilloscope was sent to the external trigger input of a pulse/delay generator (Berkeley Nucleonics Corporation, BNC 555-2). The BNC pulse generator, with its variable delay, then triggered an HP 8011A pulse generator with variable pulse width and voltage. The output voltage of the HP pulse generator was set at 16 V, and this signal directly strobed the LED array at any arbitrary phase-locked point in the oscillation cycle. The pulse width of the excitation light was set at 2.48 μs for the 9.4-kHz oscillations and 1.0 μs for the 21.0-kHz oscillations. These pulse width values are about 2.3 and 2.1% of the oscillation period, respectively. Images throughout the oscillation period were acquired, with a constant delay between data points (5-μs delay for 9.4-kHz oscillations, and 2-μs delay for 21.0-kHz oscillations). The camera exposure time for these experiments was of the order of several seconds.

Wind-on and wind-off reference images are needed for the PSP data reduction process. The wind-off reference image was divided by the particular wind-on image for each phase delay. In some cases, the ratio of the two images was then normalized to match a known value in the image region.

III. Results and Discussion

A. Water Visualization

A simple test to verify the operation of the microfluidic oscillator is to use water as the working fluid. Because the density of water is much higher than air or other gases, the operating frequency of the device is much lower. The low frequencies (of the order of several hundred hertz) facilitate visualization using simple techniques. The disadvantage of using water as a working fluid is that surface tension effects may become important to the resultant flowfield. For these tests, a digital single-lens reflex (SLR) camera with macro lens and

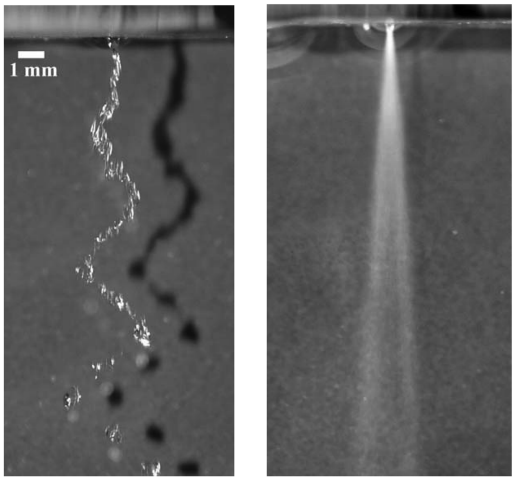

a) b)

Fig. 5 Water visualization of microfluidic oscillator flowfield: a) instantaneous (1/60 s, with flash) and b) time-averaged (1/2 s, no flash).

external flash were used to visualize the flowfield. Typical results are shown in Fig. 5a, an image captured with a flash duration of 1/500 s. The flowfield issuing from the nozzle is clearly an oscillatory waveform. The range of oscillation is several times the diameter of the jet exit (325 μm), and the width of the oscillatory pattern grows with the distance downstream of the nozzle. Figure 5b shows the oscillator at the same operating conditions, but with a longer time exposure for a time-averaged image. The sinusoidal distribution, with longer dwell times at the extrema, produces an uneven distribution of fluid in the far field, but over a wide fan angle.

B. Frequency Characteristics

The oscillation frequency of the microfluidic oscillator was evaluated across a range of flow rates. Figure 6 shows the variation of oscillation frequency with flow rate for the microfluidic oscillator. The oscillation frequency was measured by determining the frequency of the primary peak on a power spectrum of the signal from a single electret microphone (used instead of a Kulite transducer for these particular measurements). Oscillations begin at 6.0 kHz with a flow rate of 460 ml/min and increase in frequency up to 22.5 kHz with a flow rate of 1120 ml/min. The variation of frequency with flow rate is linear, but with a change in slope at 760 ml/min. The values of slope for the two linear regions are summarized in Table 1. During testing, there was a distinct change in the tone produced by the

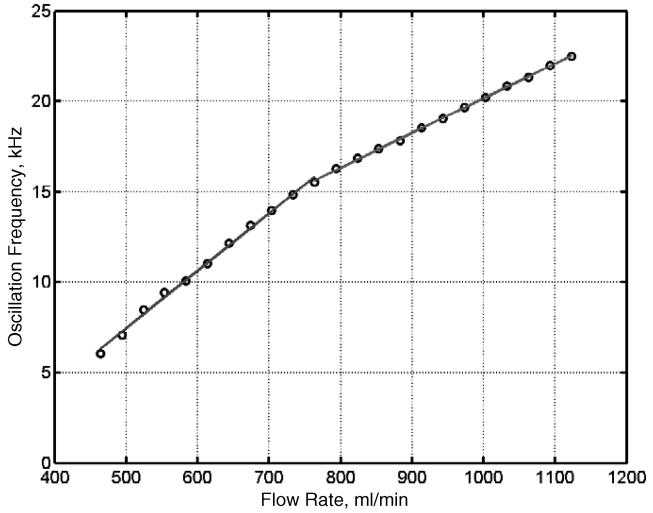

Fig. 6 Frequency characteristics of the microfluidic oscillator operated with air.

Table 1 Summary of linear dependence of oscillation frequency on flow rate

Flow rate range	Slope	Intercept
460–760 ml/min	32 Hz/(ml/min)	−8400 Hz
760–1120 ml/min	19 Hz/(ml/min)	1000 Hz

oscillator at 760 ml/min, with a simultaneous increase in the observed broadband noise. This significant increase in broadband noise is illustrated in the power spectra shown in Fig. 7. These two test conditions bracket the slope change in the frequency curve of Fig. 6 and illustrate the significant increase in broadband noise at this flow condition. The slope change in the frequency curve and the corresponding increase in broadband noise are most likely due to a transition from laminar to turbulent flow in the oscillator. Based on a jet exit diameter of 325 μm, a flow rate of 760 ml/min, and standard conditions, the Reynolds number for this test condition is 2700. This Reynolds number is fairly close to the classical transition Reynolds number for a nozzle flow, thus validating the observation that the flow has transitioned from laminar to turbulent at this flow condition. As the flow transitions, the fluid dynamics of the jet interaction within the fluidic oscillator may be altered and thus impact the frequency of oscillations. This supposition will be investigated further with the pressure-sensitive paint data.

The results in Fig. 6 show only the variation of the fundamental oscillation frequency with flow rate. The power spectrum for the oscillations is rich in higher-order frequency content, which is not revealed in Fig. 6. Thus, a frequency map was generated from Kulite pressure transducer measurements to cover the range of supply pressures and across the entire frequency spectrum, as shown in Fig. 8. Each vertical slice of this frequency map is essentially an individual power spectrum at one specific operating condition. The grayscale in the figure represents the relative magnitude within the power spectrum. Both supply pressure and volumetric flow rate were measured simultaneously, such that mass flow rate may be determined if one assumes an ideal gas and calculates density using ambient conditions (in this case, 296.6 K and 99.622 kPa). Volumetric flow rates for the abscissa of Fig. 8 range from 430 to 1240 ml/min, with corresponding mass flow rates ranging from 0.52 to 1.8 g/min. The frequency map in Fig. 8 clearly shows the primary frequency peak, beginning at just under 10 kHz and increasing to approximately 20 kHz. Higher harmonics are clearly visible all the way up to 100 kHz, particularly at the low flow rates. This indicates that the oscillations are very rich in high-frequency content. Another interesting feature visible in the frequency map is the sudden incidence of broadband noise at a supply pressure of 6.76 kPa (gauge). This can be seen on the frequency map as the sudden increase in the noise floor, indicated by a broadband discontinuity in the grayscale (an increase of approximately 10 dB). The change in the noise level may be associated with a transition from laminar to

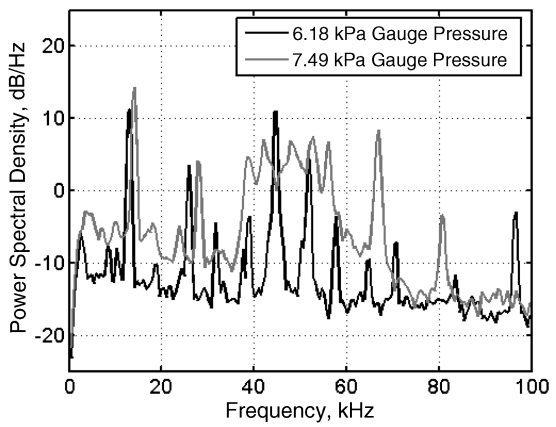

Fig. 7 Power spectra at two operating conditions that bracket the slope change in Fig. 6.

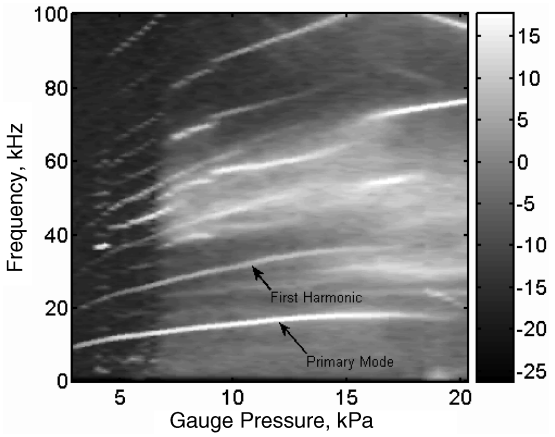

Fig. 8 Spectral map of the micro oscillator flowfield when operated with air. Each vertical slice represents the power spectrum at an individual operating condition.

turbulent flow inside the oscillator. Also noteworthy is the diminishing of the primary frequency peak at a supply pressure of about 17.7 kPa. At about the same pressure, a new high-frequency peak emerges at approximately 70 kHz. This high-frequency peak then dominates the power spectrum for higher pressures.

C. Pressure-Sensitive Paint Results

Two points on the frequency curve of Fig. 6 were chosen for further evaluation with pressure-sensitive paint. One point was chosen in the first linear region of the curve, at a low flow rate at which oscillations just begin. The second point was chosen in the other linear region, at a high flow rate near the highest oscillation frequency.

The first point corresponds to an oscillation frequency of 9.4 kHz, near the low end of the frequency range. This represents a very low flow rate [550 ml/min or ~0.67 g/ min, with a supply pressure of 6.69 kPa (gauge)]. A Kulite pressure transducer was positioned in the near field of the jet oscillations, and the time history was recorded. The power spectrum of this signal is shown in Fig. 9. Note that the spectrum is rich in higher-frequency harmonics, in addition to the fundamental frequency at 9.4 kHz. PSP data for this flow condition is shown in Figs. 10a–10c. For enhanced visualization purposes, this PSP data was acquired with nitrogen gas. Because PSP is an oxygen sensor, the nitrogen gas provides high-contrast data by purging any local atmospheric oxygen. The color scale on the PSP images ranges from pure nitrogen (dark blue) to atmospheric conditions (dark red). A photographic bellows was used with the CCD camera to create an image four times life-size on the image plane. The dimensions on the axes of the images were calibrated by imaging a scale with 100 lines per inch and determining the imaging area of each pixel. Note that the

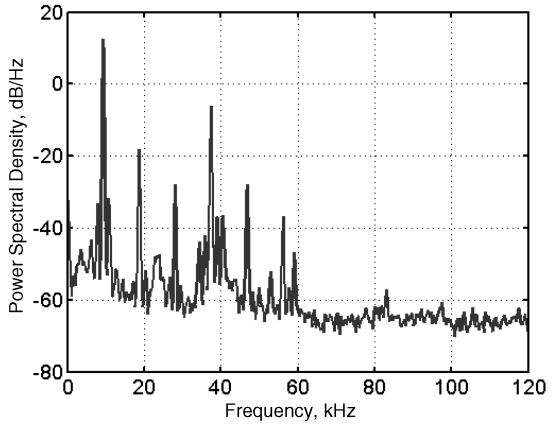

Fig. 9 Power spectrum of the pressure transducer signal, 9.4-kHz oscillations.

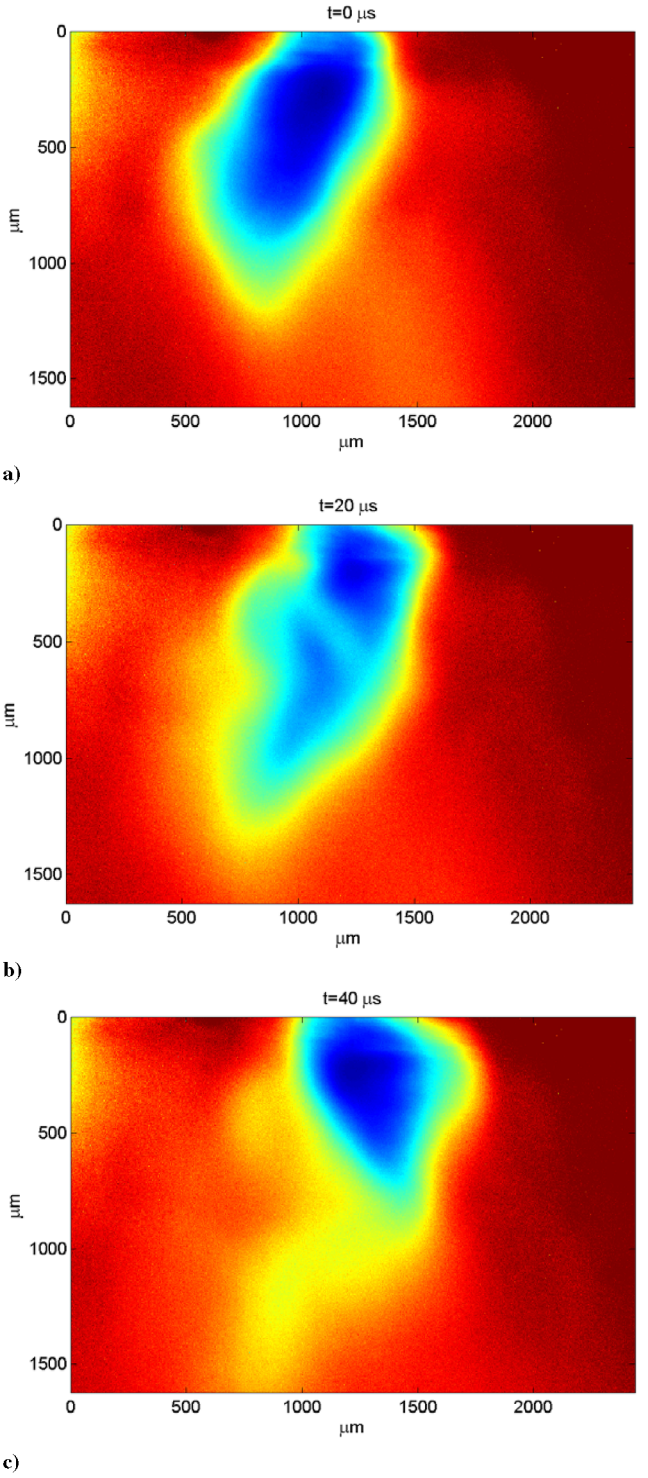

Fig. 10 Phase-averaged pressure-sensitive paint data for the microfluidic oscillator with nitrogen gas at 9.4 kHz, flow rate of 550 ml/min (~0.67 g/ min), and gauge pressure of 6.69 kPa: a) 0 μs, b) 20 μs, and c) 40 μs.

entire image area covers a region measuring approximately 2000 μm^2, with each pixel representing an area measuring 3.2 μm^2. This represents one of the smallest flowfields visualized with PSP technology, following the work of Huang, et al. [56] The data shown in Fig. 10 are phase-averaged through one period of the jet oscillation, with each image representing successive time delays from a fixed trigger. Each image is separated by 20 μs, or approximately 19% of the total cycle. These time steps were selected to represent approximately half of the oscillation period. Another representation of the same data set is shown in Fig. 11. This plot represents a horizontal cross section of the PSP data taken along a

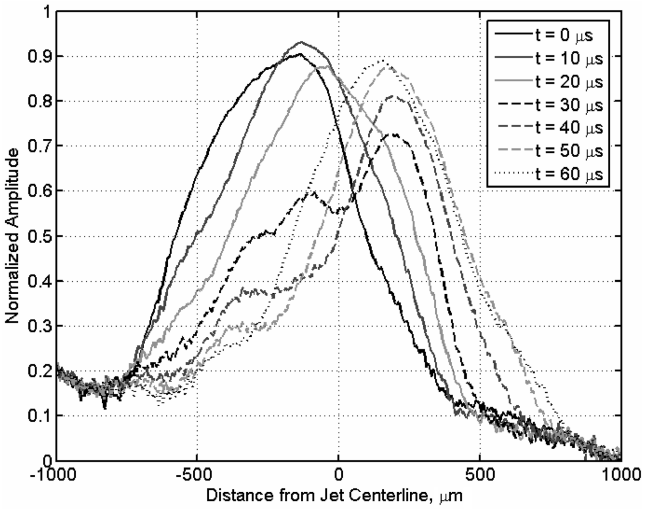

Fig. 11 Horizontal cross-sectional data taken from the PSP results at 9.4 kHz, at a location 500 μm downstream of the nozzle exit.

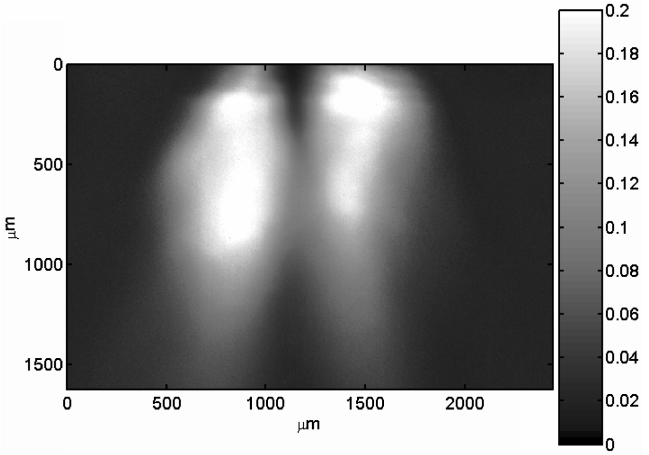

Fig. 12 RMS intensity plot from the phase-averaged time history at 9.4 kHz.

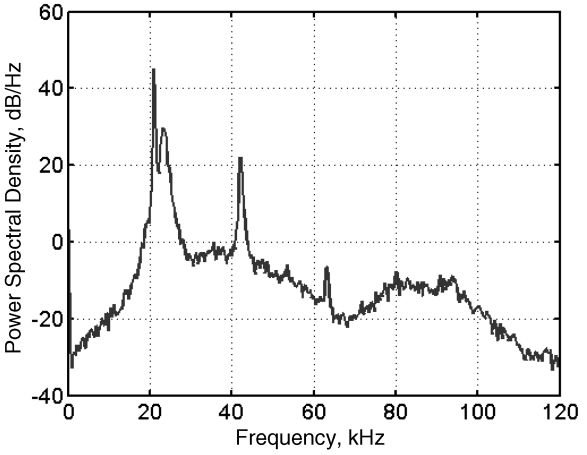

Fig. 13 Power spectrum of the pressure transducer signal, 21.0-kHz oscillations.

line 500 μm downstream of the nozzle exit. Each curve in the figure represents a successive time step of 10 μs. Notice that the jet exhibits bistable oscillatory behavior: the jet rapidly switches between the two end points. The transition time for the jet between the two extremes is very fast (of the order of 20 μs), whereas it dwells longer at the outer positions. The distance traversed by the jet between the two extremes is approximately 300 μm.

Note that the mean value on the right side of the measurement area approaches zero, whereas the mean value on the left side is approximately 0.2. This difference, which was present for all test conditions, may be attributed to imperfect alignment of the paint sample with respect to the jet exit. Despite this observation, paint intrusiveness effects are considered minimal, as justified by the following rationale. First, the PSP sample was positioned such that no part of the paint sample obstructed the jet orifice. This was evaluated by monitoring the flow rate through the device while positioning the paint sample on a fine-resolution traverse. The PSP was positioned as close to the jet exit as possible, without altering the flow rate or pressure conditions. Second, the frequency of oscillations was recorded with and without the paint sample being present. There was no discernible variation in oscillation frequency, whether or not the PSP was in position. Third, the effects of plate angle with respect to the jet oscillation plane are considered. The angle of the plate is the most difficult geometric parameter to control, yet the effects on the flowfield are deemed marginal. The peak value of the oscillations at both extremes of the jet motion in Fig. 11 differs by only 4.4%. Assuming the jet oscillations are symmetric about the vertical axis, this indicates that errors due to the plate angle are less than 5%. Thus, the intrusive effects of the PSP sample on the flowfield are considered negligible.

Another indicator of the jet oscillation characteristics is the RMS intensity plot shown in Fig. 12. For each pixel location, a phase-averaged time-history is generated from the PSP intensity data. The root-mean-square value of the fluctuations is calculated for each point in the flow, as shown in Fig. 12. This figure indicates that there is a two-lobed region of high fluctuations, with the area near the jet centerline being relatively constant. This supports the bimodal observation of the jet oscillations. The slight asymmetry visible between the two lobes is most likely due to imperfect alignment of the PSP with respect to the nozzle.

The second operating point corresponds to an oscillation frequency of 21.0 kHz, near the high end of the frequency range. This corresponds to a flow rate of 1170 ml/min ($\sim$1.9 g/ min) and a supply pressure of 44.5 kPa (gauge). The power spectrum of this signal from the Kulite pressure transducer is shown in Fig. 13. Note that the spectrum has fewer high-frequency harmonics than the 9.4-kHz power spectrum (Fig. 9), indicating that these flow oscillations are more closely sinusoidal than the oscillations at the 9.4-kHz case. PSP data for the 21.0-kHz condition are shown in Figs. 14a and 14b. The images are separated by 18 μs, or approximately 38% of the total cycle. These time steps were selected to represent approximately half of the oscillation period. The data presented in Fig. 14 represent one of the fastest oscillatory flowfields measured to date with PSP. Even though the jet is oscillating at a rate of 21.0 kHz, there are no visible effects of frequency rolloff in the PSP measurements. If the period of the fluidic oscillations was shorter than the time response of the paint, then the data would show significantly reduced values of the jet gas concentration (as illustrated by Gregory and Sullivan [35]). Also, the shape of the oscillating jet is fairly straight, compared with the shape of the 9.4-kHz jet shown in Fig. 10c. The fundamental characteristics of the oscillations at high flow rates are significantly different from the low flow characteristics. A series of horizontal cross-sectional lines from the PSP data at successive time steps is shown in Fig. 15. The amplitude of the jet remains fairly constant throughout the cycle, unlike the results shown in Fig. 11. Furthermore, the jet oscillates in a uniform, consistent manner that reflects its sinusoidal nature. The range of motion of the jet in this case is approximately 200 μm, compared with 300 μm for the 9.4-kHz case. Despite having a narrower range of oscillatory motion than the lower frequency case, the range of influence at this high-frequency condition is quite remarkable. The jet traverse distance remains a significant percentage of the total jet width ($\sim$325 μm). This wide region of impact over a large range of frequencies is a compelling feature of the oscillator when applied to flow control problems.

The RMS intensity profile for the 21.0-kHz oscillations is shown in Fig. 16. This plot is similar to Fig. 12, except that the magnitude of the fluctuations is much less. Finally, notice that the nature of the oscillations for this 21-kHz flow condition is much closer to

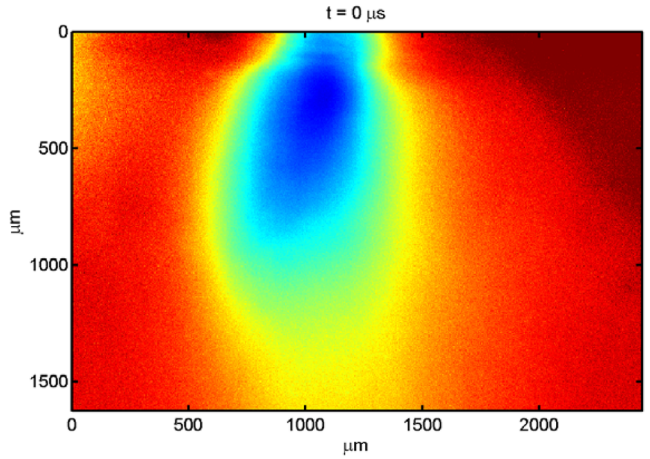

a)

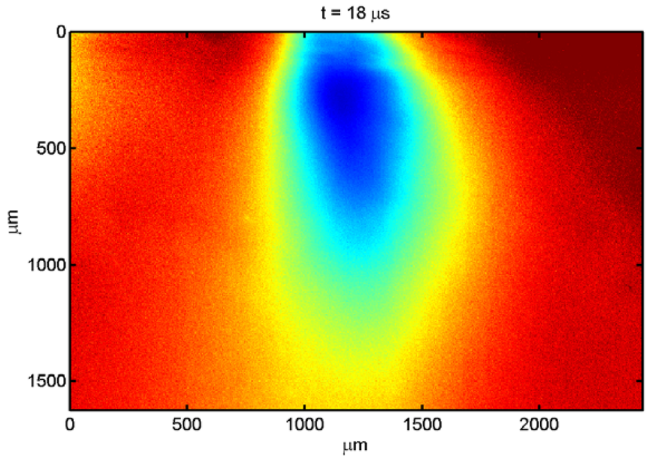

b)

Fig. 14 Phase-averaged pressure-sensitive paint data for the microfluidic oscillator with nitrogen gas at 21.0 kHz, flow rate of 1170 ml/min (∼1.9 g/min), and gauge pressure of 44.5 kPa: a) 0 μs and b) 18 μs.

sinusoidal. A detailed comparison of the signal time histories, derived from the time-resolved PSP data, is shown in for both the 9- and 21-kHz conditions in Fig. 17. The 9-kHz oscillations produce a triangular waveform, whereas the 21-kHz oscillations produce a nearly sinusoidal waveform. The nature of the waveforms is also illustrated in the normalized power spectra in Fig. 18. The magnitudes of the frequency peaks for the higher harmonics of the

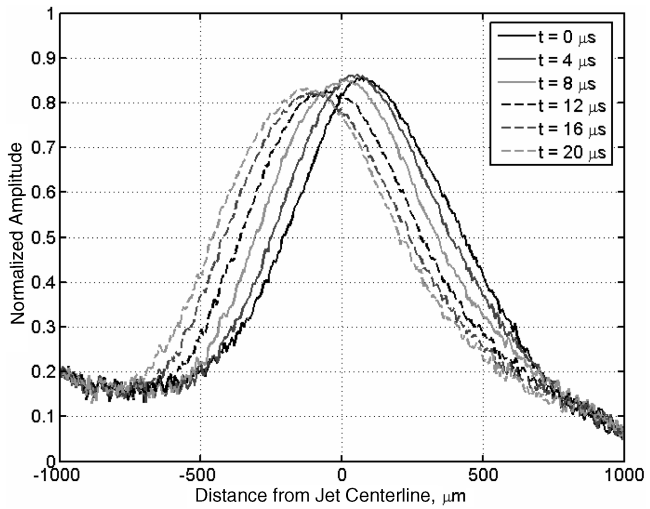

Fig. 15 Horizontal cross-sectional data taken from the PSP results at 21.0 kHz, at a location 500 μm downstream of the nozzle exit.

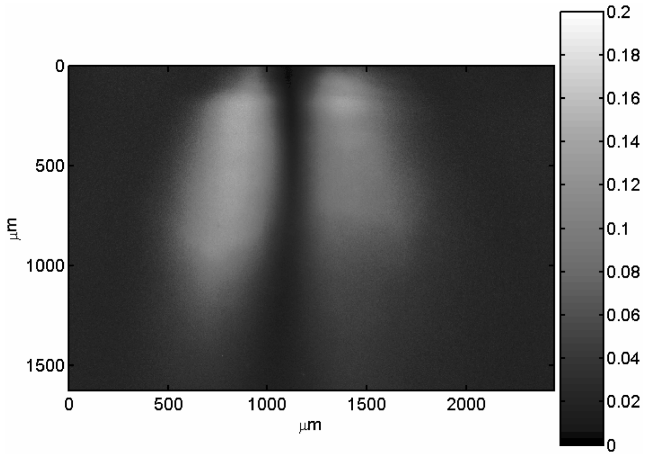

Fig. 16 RMS Intensity plot from the phase-averaged time history at 21.0 kHz.

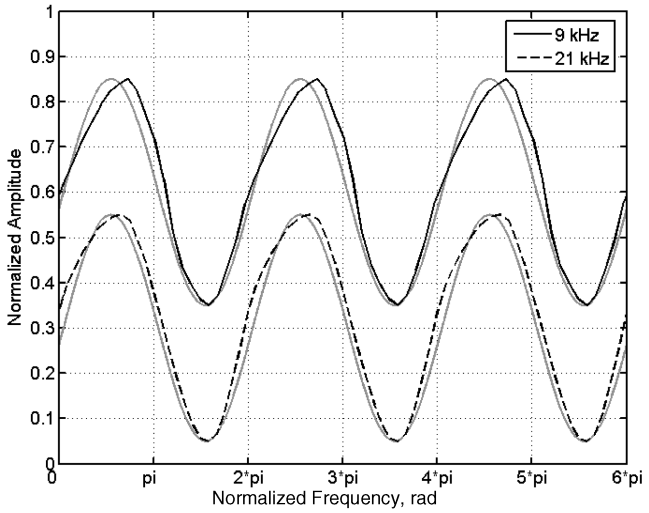

Fig. 17 Normalized time histories of the oscillatory waveform, derived from PSP data at 9 and 21 kHz, and compared with pure sine waves.

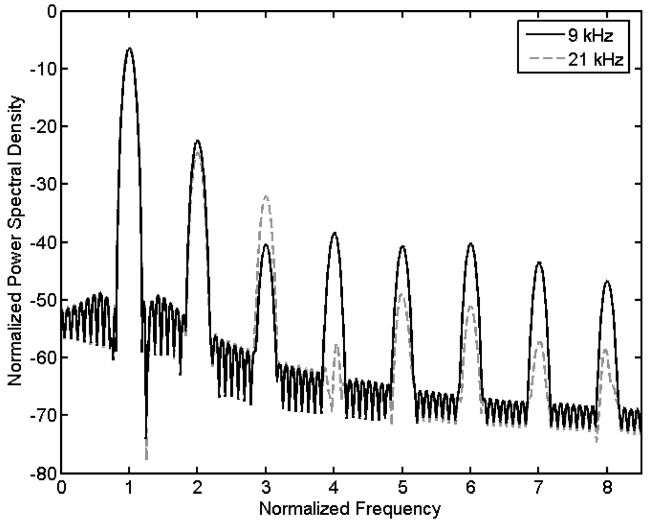

Fig. 18 Normalized power spectra for the 9- and 21-kHz oscillations, as measured by PSP.

21-kHz case are lower than the peaks for the 9-kHz case, indicating that the waveform is more sinusoidal. These observations correlate well with the harmonic content of the power spectra shown in Figs. 9 and 13.

The first set of PSP data represents flow conditions in the lower linear region of Fig. 6, and the second set of PSP data represents the

higher linear region. It is clear that the oscillatory flowfield has changed significantly between these two flow conditions. The change in the external flowfield characteristics is most likely correlated with the increase in broadband noise and slope discontinuity in the frequency response at a flow rate of 760 ml/min. These characteristics are an indicator of a transition of the internal fluid dynamics between operating regimes, most likely a transition from laminar to turbulent flow that coincides with the slope change in the frequency curve. These characteristics of the microfluidic oscillator mirror the characteristics of larger fluidic oscillators of the same design. Despite the disparity in length scales, larger fluidic oscillators also demonstrate the transition phenomenon at similar Reynolds numbers [26].

IV. Conclusions

The microfluidic oscillator is an excellent candidate for use as a flow control actuator. The fluidic device produces an unsteady jet that oscillates at frequencies from 6 to 22 kHz. These particular micro oscillators require only very small flow rates: of the order of 1 l/ min ($\sim$1 g/ min). A distinguishing characteristic of the fluidic oscillator as a flow control actuator is that it spatially modulates the flow in a time-varying manner, as opposed to a typical pulsed jet. One of the most significant advantages of the fluidic oscillator is its simplicity. Fluidic oscillations are generated purely by fluid dynamic phenomena; thus, the lack of moving parts makes the micro oscillator attractive as a practical excitation device. Microfluidic oscillators may be implemented for flow control applications in which high frequencies and low flow rates are required.

As such, the flowfield of the microfluidic oscillator needed to be characterized. This work used porous pressure-sensitive paint to make time-resolved full-unsteady measurements of the jet oscillations. In addition, microphones and Kulite pressure transducers were used to characterize the power spectra at various operating conditions. Water flow was also used to visualize the instantaneous and time-averaged behavior of the micro oscillator.

The dependence of frequency on flow rate was evaluated and found to range from 6 kHz to over 22 kHz, corresponding to flow rates of about 400 to 1100 ml/min. Interestingly, the variation of frequency with flow rate was found to be linear, except at one distinct slope discontinuity in which the turbulent noise increased dramatically. The oscillations above and below this slope discontinuity were shown to exhibit different characteristics. Oscillations at points below the discontinuity were similar to a triangular wave, with rich high-frequency content. Oscillations above the discontinuity, however, were nearly sinusoidal, as shown by PSP data and power spectra.

Finally, this work demonstrated the utility of pressure-sensitive paint as a measurement technique for high-frequency and small-scale flowfields. The PSP system was used to study a flowfield oscillating at frequencies up to 21 kHz, with a spatial resolution as fine as 3 μm per pixel. This instrumentation provided time-history data at over 393,000 points within a 1.5×2.3 mm area.

Acknowledgments

J. W. Gregory thanks the NASA Graduate Student Researchers Program (GSRP), which provided funding for this work. The authors would also like to thank Hirotaka Sakaue for his work in preparing the anodized aluminum PSP sample used in these experiments.

References

[1] Glezer, A., and Amitay, M., "Synthetic Jets," *Annual Review of Fluid Mechanics*, Vol. 34, 2002, pp. 503–529.

[2] Wiltse, J. M., and Glezer, A., "Direct Excitation of Small-Scale Motions in Free Shear Flows," *Physics of Fluids*, Vol. 10, No. 8, 1998, pp. 2026–2036.

[3] Wiltse, J. M., and Glezer, A., "Manipulation of Free Shear Flows Using Piezoelectric Actuators," *Journal of Fluid Mechanics*, Vol. 249, Apr. 1993, pp. 261–285.

[4] Raman, G., Khanafseh, S., Cain, A. B., and Kerschen, E., "Development of High Bandwidth Powered Resonance Tube Actuators with Feedback Control," *Journal of Sound and Vibration*, Vol. 269, Nos. 3–5, 2004, pp. 1031–1062.

[5] Kastner, J., and Samimy, M., "Development and Characterization of Hartmann Tube Fluidic Actuators for High-Speed Flow Control," *AIAA Journal*, Vol. 40, No. 10, 2002, pp. 1926–1934.

[6] Gregory, J. W., and Sullivan, J. P., "Characterization of Hartmann Tube Flow with Porous Pressure-Sensitive Paint," 33rd Fluid Dynamics Conference, Orlando, FL, AIAA Paper 2003-3713, 2003.

[7] Roth, J. R., Sherman, D. M., and Wilkinson, S. P., "Electrohydrodynamic Flow Control with a Glow-Discharge Surface Plasma," *AIAA Journal*, Vol. 38, No. 7, 2000, pp. 1166–1172.

[8] Enloe, C. L., McLaughlin, T. E., VanDyken, R. D., Kachner, K. D., Jumper, E. J., and Corke, T. C., "Mechanisms and Responses of a Single Dielectric Barrier Plasma Actuator: Plasma Morphology," *AIAA Journal*, Vol. 42, No. 3, 2004, pp. 589–594.

[9] Enloe, C. L., McLaughlin, T. E., VanDyken, R. D., Kachner, K. D., Jumper, E. J., Corke, T. C., Post, M., and Haddad, O., "Mechanisms and Responses of a Single Dielectric Barrier Plasma Actuator: Geometric Effects," *AIAA Journal*, Vol. 42, No. 3, 2004, pp. 595–604.

[10] Post, M., and Corke, T. C., "Separation Control on High Angle of Attack Airfoil Using Plasma Actuators," *AIAA Journal*, Vol. 42, No. 11, 2004, pp. 2177–2184.

[11] Magill, J. C., and McManus, K. R., "Exploring the Feasibility of Pulsed Jet Separation Control for Aircraft Configurations," *Journal of Aircraft*, Vol. 38, No. 1, 2001, pp. 48–56.

[12] M'Closkey, R. T., King, J. M., Cortelezzi, L., and Karagozian, A. R., "The Actively Controlled Jet in Crossflow," *Journal of Fluid Mechanics*, Vol. 452, 2002, pp. 325–335.

[13] Chiekh, M. B., Bera, J. C., Michard, M., Comte-Bellot, G., and Sunyach, M., "Control of a Plane Jet by Fluidic Wall Pulsing," *AIAA Journal*, Vol. 41, No. 5, 2003, pp. 972–975.

[14] Rao, N. M., Feng, J., Burdisso, R. A., and Ng, W. F., "Experimental Demonstration of Active Flow Control to Reduce Unsteady Stator-Rotor Interaction," *AIAA Journal*, Vol. 39, No. 3, 2001, pp. 458–464.

[15] Saric, W. S., and Reed, H. L., "Effect of Suction and Weak Mass Injection on Boundary-Layer Transition," *AIAA Journal*, Vol. 24, No. 3, 1986, pp. 383–389.

[16] Morris, N. M., *An Introduction to Fluid Logic*, McGraw–Hill, London, 1973, pp. 58–66.

[17] Kirshner, J. M., and Katz, S., *Design Theory of Fluidic Components*, Academic Press, New York, 1975.

[18] Raber, R. A., and Shinn, J. N. (eds.), "Fluid Amplifier State of the Art, Vol. 1: Research and Development, Fluid Amplifiers and Logic," NASA Contractor Rept. CR-101, Oct. 1964.

[19] Raber, R. A., and Shinn, J. N. (eds.), "Fluid Amplifier State of the Art, Vol. 2: Bibliography," NASA Contractor Rept. CR-102, Oct. 1964.

[20] Spyropoulos, C. E., "A Sonic Oscillator," *Proceedings of the Fluid Amplification Symposium*, Vol. 3, Harry Diamond Labs., Washington, D.C., 1964, pp. 27–51.

[21] Viets, H., "Flip-Flop Jet Nozzle," *AIAA Journal*, Vol. 13, No. 10, 1975, pp. 1375–1379.

[22] Stouffer, R. D., "Liquid Oscillator Device," U.S. Patent 4,508,267, filed 2 Apr. 1985.

[23] Shakouchi, T., "Fluidic Oscillator Operated by Gas(Air)-Liquid(Water) Two-Phase Flow (Measurement of Flow Rate of Gas-Liquid Two-Phase Flow in Pipe)," *Proceedings of the ASME Fluids Engineering Division Summer Meeting*, Vol. 1, American Society of Mechanical Engineers, New York, 2001, pp. 895–901.

[24] Wang, H., Beck, S. B. M., Priestman, G. H., and Boucher, R. F., "Fluidic Pressure Pulse Transmitting Flowmeter," *Chemical Engineering Research and Design: Transactions of the Institute of Chemical Engineers*, Part A, Vol. 75, No. A4, 1997, pp. 381–391.

[25] Raman, G., and Raghu, S., "Cavity Resonance Suppression Using Miniature Fluidic Oscillators," *AIAA Journal*, Vol. 42, No. 12, 2004, pp. 2608–2611.

[26] Gregory, James, W., "Development of Fluidic Oscillators as Flow Control Actuators," Ph.D. Dissertation, School of Aeronautics and Astronautics, Purdue Univ., West Lafayette, IN, 2005.

[27] Raman, G., Hailye, M., and Rice, E. J., "Flip-Flop Jet Nozzle Extended to Supersonic Flows," *AIAA Journal*, Vol. 31, No. 6, 1993, pp. 1028–1035.

[28] Raman, G., "Using Controlled Unsteady Fluid Mass Addition to Enhance Jet Mixing," *AIAA Journal*, Vol. 35, No. 4, 1997, pp. 647–656.

[29] Raman, G., and Cornelius, D., "Jet Mixing Control Using Excitation from Miniature Oscillating Jets," *AIAA Journal*, Vol. 33, No. 2, 1995, pp. 365–368.

[30] Raman, G., Packiarajan, S., Papadopoulos, G., Weissman, C., and Raghu, S., "Jet Thrust Vectoring Using a Miniature Fluidic Oscillator," *Proceedings of the ASME Fluids Engineering Division Summer*

Meeting, Vol. 1, American Society of Mechanical Engineers, New York, 2001, pp. 903–913; also American Society of Mechanical Engineers, Fluids Engineering Div., Paper 2001-18057.

[31] Cerretelli, C., and Kirtley, K., "Boundary Layer Separation Control with Fluidic Oscillators," American Society of Mechanical Engineers Paper GT2006-90738, 2006.

[32] Raman, G., Rice, E. J., and Cornelius, D. M., "Evaluation of Flip-Flop Jet Nozzles for Use as Practical Excitation Devices," *Journal of Fluids Engineering*, Vol. 116, No. 3, 1994, pp. 508–515.

[33] Raghu, S., and Raman, G., "Miniature Fluidic Devices for Flow Control," American Society of Mechanical Engineers, Fluids Engineering Div., Paper 99-7526, 1999.

[34] Sakaue, H., Gregory, J. W., Sullivan, J. P., and Raghu, S., "Porous Pressure-Sensitive Paint for Characterizing Unsteady Flowfields," *AIAA Journal*, Vol. 40, No. 6, 2002, pp. 1094–1098.

[35] Gregory, J. W., and Sullivan, J. P., "Effect of Quenching Kinetics on Unsteady Response of Pressure-Sensitive Paint," *AIAA Journal*, Vol. 44, No. 3, 2006, pp. 634–645.

[36] Gregory, J. W., Sakaue, H., and Sullivan, J. P., "Fluidic Oscillator as a Dynamic Calibration Tool," 22nd Aerodynamic Measurement Technology and Ground Testing Conference, St. Louis, MO, AIAA Paper 2002-2701, 2002.

[37] Gregory, J. W., "Porous Pressure-Sensitive Paint for Measurement of Unsteady Pressures in Turbomachinery," 42nd Aerospace Sciences Meeting, Reno, NV, AIAA Paper 2004-0294, 2004.

[38] Gregory, J. W., Sullivan, J. P., and Raghu, S., "Visualization of Jet Mixing in a Fluidic Oscillator," *Journal of Visualization*, Vol. 8, No. 2, 2005, pp. 169–176.

[39] Raghu, Surya, "Feedback-Free Fluidic Oscillator and Method," U.S. Patent 6,253,782, filed 3 July 2001.

[40] Peterson, J. I., and Fitzgerald, R. V., "New Technique of Surface Flow Visualization Based on Oxygen Quenching of Fluorescence," *Review of Scientific Instruments*, Vol. 51, No. 5, 1980, pp. 670–671.

[41] Kavandi, J., Callis, J., Gouterman, M., Khalil, G., Wright, D., Green, E., Burns, D., and McLachlan, B., "Luminescent Barometry in Wind Tunnels," *Review of Scientific Instruments*, Vol. 61, No. 11, 1990, pp. 3340–3347.

[42] Bell, J. H., Schairer, E. T., Hand, L. A., and Mehta, R. D., "Surface Pressure Measurements Using Luminescent Coatings," *Annual Review of Fluid Mechanics*, Vol. 33, 2001, pp. 155–206.

[43] Liu, T., and Sullivan, J. P., *Pressure and Temperature Sensitive Paints*, Springer, New York, 2005.

[44] Sakaue, Hirotaka, "Anodized Aluminum Pressure Sensitive Paint for Unsteady Aerodynamic Applications," Ph.D. Dissertation, School of Aeronautics and Astronautics, Purdue Univ., West Lafayette, IN, 2003.

[45] Asai, K., Iijima, Y., Kanda, H., and Kunimasu, T., "Novel Pressure-Sensitive Coating Based on Anodic Porous Alumina," *30th Fluid Dynamics Conference*, Japan Society for Aeronautical and Space Sciences, Okayama, Japan, 1998, pp. 357–360 (in Japanese).

[46] Asai, K., Amao, Y., Iijima, Y., Okura, I., and Nishide, H., "Novel Pressure-Sensitive Paint for Cryogenic and Unsteady Wind Tunnel Testing," 21st Aerodynamic Measurement Technology and Ground Testing Conference, Denver, CO, AIAA Paper 2000-2527, 2000.

[47] Teduka, N., Kameda, M., Amao, Y., and Asai, K., "Experimental Investigation on the Time Response of Pressure-Sensitive Paint," *Proceedings of the 31st JSASS Annual Meeting*, Japan Society for Aeronautical and Space Sciences, Tokyo, Japan, 2000, pp. 218–221 (in Japanese).

[48] Sakaue, H., and Sullivan, J. P., "Time Response of Anodized Aluminum Pressure-Sensitive Paint," *AIAA Journal*, Vol. 39, No. 10, 2001, pp. 1944–1949.

[49] Sakaue, H., Sullivan, J. P., Asai, K., Iijima, Y., and Kunimasu, T., "Anodized Aluminum Pressure Sensitive Paint in a Cryogenic Wind Tunnel," *Proceedings of the 45th International Instrumentation Symposium*, Instrument Society of America, Research Triangle Park, NC, 1999, pp. 337–346.

[50] Baron, A. E., Danielson, J. D. S., Gouterman, M., Wan, J. R., Callis, J. B., and McLachlan, B., "Submillisecond Response Times of Oxygen-Quenched Luminescent Coatings," *Review of Scientific Instruments*, Vol. 64, No. 12, 1993, pp. 3394–3402.

[51] Scroggin, A. M., Slamovich, E. B., Crafton, J. W., Lachendro, N., and Sullivan, J. P., "Porous Polymer/Ceramic Composites for Luminescence-Based Temperature and Pressure Measurement," *Materials Research Society Symposium Proceedings*, Vol. 560, Materials Research Society, Warrendale, PA, 1999, pp. 347–352.

[52] Scroggin, Aaron, M., "Processing and Optimization of Doped Polymer/Ceramic Composite Films for Luminescence-Based Pressure and Temperature Measurement in Aerodynamic Applications," M.S. Thesis, School of Materials Engineering, Purdue Univ., West Lafayette, IN, 1999.

[53] Gregory, James, W., "Unsteady Pressure Measurements in a Turbocharger Compressor Using Porous Pressure-Sensitive Paint," M.S. Thesis, School of Aeronautics and Astronautics, Purdue Univ., West Lafayette, IN, 2002.

[54] Gregory, J. W., Sullivan, J. P., Wanis, S., and Komerath, N. M., "Pressure-Sensitive Paint as a Distributed Optical Microphone Array," *Journal of the Acoustical Society of America*, Vol. 119, No. 1, 2006, pp. 251–261.

[55] Asai, K., Nakakita, K., Kameda, M., and Teduka, K., "Recent Topics in Fast-Responding Pressure-Sensitive Paint Technology at National Aerospace Laboratory," *ICIASF'01: 19th International Congress on Instrumentation in Aerospace Simulation Facilities*, Inst. of Electrical and Electronics Engineers, Piscataway, NJ, 2001, pp. 25–36.

[56] Huang, C. Y., Sakaue, H., Gregory, J. W., and Sullivan, J. P., "Molecular Sensors for MEMS," 40th Aerospace Sciences Meeting, Reno, NV, AIAA Paper 2002-0256, 2002.

F. Coton
Associate Editor